

Enlarging a photonic band gap by using insertion

Xiangdong Zhang, Zhao-Qing Zhang, and Lie-Ming Li

Department of Physics, Hong Kong University of Science and Technology, Clear Water Bay, Kowloon, Hong Kong, China

C. Jin, D. Zhang, B. Man, and B. Cheng

Institute of Physics, Chinese Academy of Sciences, P.O. Box 603, Beijing, China

(Received 29 July 1999)

We propose a simple, systematic, and efficient method to enlarge the gap of a photonic crystal. In this method, we add a small fraction of a third component into the existing photonic crystal. The dielectric property of the third component as well as its insertion position in a unit cell are chosen according to the field-energy distribution of two Bloch states at the band edges. The method is very general. It can be applied to any microstructure and is independent of the dimensionality of the original photonic crystal. Thus, it opens up a way to engineer photonic band gaps. Here, we demonstrate the validity of this method explicitly in two dimensions for both s and p waves. We show that, for certain microstructures, absolute gaps can be significantly enlarged. The method is also demonstrated in microwave experiments.

I. INTRODUCTION

During the past few years, a significant effort has been devoted to the study of photonic crystals.¹⁻¹⁴ The existence of gaps, which prohibit the propagation of electromagnetic (EM) waves in any direction, provides an opportunity to confine and control the propagation of EM waves. It can have profound implications for quantum optics, high-efficiency lasers, optoelectronic devices, and other areas of applications.^{1,9} Various photonic band-gap (PBG) structures have been successfully fabricated in two and three dimensions (2D and 3D) for frequencies in both microwave and near-infrared regions.³⁻⁸ Despite the progress that has been made in the application and fabrication of photonic crystals, the search for new microstructures that can produce larger gaps remains to be the important issue. The creation of a gap depends on many factors in the microstructure such as topology, dielectric contrast ratio, lattice structure, and filling factor. The dielectric contrast ratio is often limited by material properties and causes a severe constraint to the search for photonic crystals with large gaps, particularly in the technologically important near-infrared region. In order to have large dielectric contrast, metallic (or metallodielectric) photonic crystals (MPC's) have also been studied.⁹⁻¹³ Although large gaps have been achieved in MPC's, they also suffer from absorption, which becomes more important in the optical regime. Recently, by using the plane-wave expansion technique, Anderson and Giapis have shown in 2D that the absolute gap can be increased by reducing the structural symmetry.¹⁴ Although some higher-order gap is enhanced, the lower-order gap is often reduced as a result of symmetry breaking. This leads us to the question of if we can have a generic method that allows us to enlarge any gap by altering the microstructure of the original photonic crystal.

In this paper, we propose a simple, systematic, and efficient method to enlarge a gap by adding a small fraction of third component into the system. In this method, we combine perturbation analysis and the multiple-scattering calculations. For any given gap, the perturbation analysis provides

us the guide in choosing the dielectric property of the third component as well as its insertion position in a unit cell. The gap structure of the altered microstructure will be calculated by using the multiple-scattering method. Our method is very general. It does not require symmetry breaking. It can be applied to any microstructure and is independent of the dimensionality of the original PBG system. Thus, it opens up a way to engineer PBG's. In the case of a metallic third component, significant gap enhancement can be achieved. However, due to its small filling factor, absorption will not be significant even in the optical regime. The outline of this paper is as follows. Our perturbative approach is described in Sec. II. The numerical results for both the perturbative and multiple-scattering approaches are given in Sec. III. In Sec. IV, an experimental demonstration of our method is presented. A conclusion is given in Sec. V.

II. THE PERTURBATIVE APPROACH

For a periodic dielectric constant $\epsilon(\mathbf{r})$, a Bloch state for the magnetic field at the n th band and wave vector \vec{k} satisfies the Maxwell equation

$$c^2 \nabla \times [\epsilon^{-1}(\mathbf{r}) \nabla \times \mathbf{H}_{n\mathbf{k}}(\mathbf{r})] = \omega_{n\mathbf{k}}^2 \mathbf{H}_{n\mathbf{k}}(\mathbf{r}), \quad (1)$$

where the eigenfrequencies $\omega_{n\mathbf{k}}$ give the band structures.² Let us denote $\bar{\epsilon}(\mathbf{r})$, $\bar{\omega}_{n\mathbf{k}}$, and $\mathbf{H}_{n\mathbf{k}}(\mathbf{r}) + \delta\mathbf{H}_{n\mathbf{k}}(\mathbf{r})$, respectively, as the new dielectric constant, eigenfrequency, and eigenfield after the insertion of a third component. If we ignore the higher-order term, from perturbation theory, it is easy to see from Eq. (1) that

$$\begin{aligned} \nabla \times \left(\frac{1}{\epsilon(\mathbf{r})} \right) \nabla \times \delta\mathbf{H}_{n\mathbf{k}} + \nabla \times \left(\frac{1}{\bar{\epsilon}(\mathbf{r})} - \frac{1}{\epsilon(\mathbf{r})} \right) \nabla \times \mathbf{H}_{n\mathbf{k}} \\ \cong \frac{\bar{\omega}_{n\mathbf{k}}^2 - \omega_{n\mathbf{k}}^2}{c^2} \mathbf{H}_{n\mathbf{k}} + \frac{\omega_{n\mathbf{k}}^2}{c^2} \delta\mathbf{H}_{n\mathbf{k}}. \end{aligned} \quad (2)$$

By multiplying both sides of Eq. (2) by $\mathbf{H}_{n\mathbf{k}}^*$ and integrating over a unit cell, we find

$$\begin{aligned}
& \int \frac{1}{\epsilon(\mathbf{r})} (\nabla \times \mathbf{H}_{n\mathbf{k}}^*) \cdot (\nabla \times \delta \mathbf{H}_{n\mathbf{k}}) d\mathbf{r} + \int \left(\frac{1}{\tilde{\epsilon}(\mathbf{r})} - \frac{1}{\epsilon(\mathbf{r})} \right) \\
& \quad \times |\nabla \times \mathbf{H}_{n\mathbf{k}}|^2 d\mathbf{r} \\
& \cong \frac{\tilde{\omega}_{n\mathbf{k}}^2 - \omega_{n\mathbf{k}}^2}{c^2} \int |\mathbf{H}_{n\mathbf{k}}|^2 d\mathbf{r} + \frac{\omega_{n\mathbf{k}}^2}{c^2} \\
& \quad \times \int (\delta \mathbf{H}_{n\mathbf{k}} \cdot \mathbf{H}_{n\mathbf{k}}^*) d\mathbf{r}. \quad (3)
\end{aligned}$$

However, from Eq. (1), we also have

$$\begin{aligned}
& \int \left(\frac{1}{\epsilon(\mathbf{r})} \right) \nabla \times \delta \mathbf{H}_{n\mathbf{k}} \cdot \nabla \times \mathbf{H}_{n\mathbf{k}}^*(\mathbf{r}) d\mathbf{r} \\
& = \frac{\omega_{n\mathbf{k}}^2}{c^2} \int \delta \mathbf{H}_{n\mathbf{k}} \cdot \mathbf{H}_{n\mathbf{k}}^*(\mathbf{r}) d\mathbf{r}. \quad (4)
\end{aligned}$$

By substituting Eq. (4) into Eq. (3), and using the displacement field

$$\mathbf{D}_{n\mathbf{k}}(\mathbf{r}) = (-ic/\omega_{n\mathbf{k}}) \nabla \times \mathbf{H}_{n\mathbf{k}}(\mathbf{r})$$

as well as the relation

$$\int |\mathbf{H}_{n\mathbf{k}}(\mathbf{r})|^2 d\mathbf{r} = \int \epsilon^{-1}(\mathbf{r}) |\mathbf{D}_{n\mathbf{k}}(\mathbf{r})|^2 d\mathbf{r},$$

we finally obtain

$$\left(\frac{\tilde{\omega}_{n\mathbf{k}}}{\omega_{n\mathbf{k}}} \right)^2 - 1 \approx \frac{\int [\tilde{\epsilon}^{-1}(\mathbf{r}) - \epsilon^{-1}(\mathbf{r})] |\mathbf{D}_{n\mathbf{k}}(\mathbf{r})|^2 d\mathbf{r}}{\int \epsilon^{-1}(\mathbf{r}) |\mathbf{D}_{n\mathbf{k}}(\mathbf{r})|^2 d\mathbf{r}}. \quad (5)$$

The function $\tilde{\epsilon}^{-1}(\mathbf{r}) - \epsilon^{-1}(\mathbf{r})$ is nonzero, say δ , only at the insertion position. We would like to point out that the similar formula has been derived by Joannopoulos, Meade, and Winn in discussing the defect states in PBG materials.² Equation (5) provides a simple way to estimate the shift in eigenfrequency before and after the insertion. For two Bloch states at the band edges of the gap, we denote the shifts as $\Delta\omega_l = \tilde{\omega}_{nL} - \omega_{nL}$ and $\Delta\omega_u = \tilde{\omega}_{mU} - \omega_{mU}$, where L and U represent the symmetry points of the band structures at the lower and upper edges of the gap, respectively. The sign of $\Delta\omega_l$ or $\Delta\omega_u$ depends on that of δ . It is their relative change, $\Delta\omega_g = \Delta\omega_u - \Delta\omega_l$, that determines the enlargement or reduction of the gap. The value of $\Delta\omega_g$ can be positive or negative, depending sensitively on the difference in the field-energy distribution of the two states at the band edges as well as the insertion position. For instance, if the minimum of $|D_{nL}|^2$ occurs at the same position as the maximum of $|D_{mU}|^2$, an optimal enlargement of the gap can be achieved by inserting a third component with positive δ at this position. A negative δ can also enhance the gap if $|D_{nL}|^2$ is at the maximum at the insertion position, whereas $|D_{mU}|^2$ is at the minimum. Thus, Eq. (5) provides a useful guide for the engineering of a gap by using insertion as a new degree of freedom.

For s waves, we consider 2D structure consisting of infinite-length parallel cylinders. We use the electric field

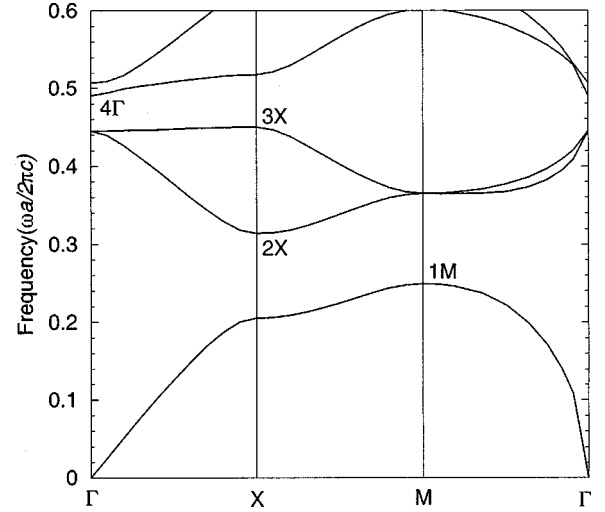


FIG. 1. Calculated photonic band structure of s wave for a square lattice of an air cylinder with $R/a=0.485$. The dielectric constant of background is taken as 11.4.

$[E_{n\mathbf{k}}(\mathbf{r})]$ that is parallel to the cylinder axis to describe a Bloch state, and the Maxwell equation in a scalar form can be written as

$$[c^{-2}\omega_{n\mathbf{k}}^2\epsilon(\mathbf{r}) + \nabla^2]E_{n\mathbf{k}}(\mathbf{r}) = 0. \quad (6)$$

Similar to the above p wave, the perturbation theory now gives

$$\left(\frac{\tilde{\omega}_{n\mathbf{k}}}{\omega_{n\mathbf{k}}} \right)^2 - 1 \approx \frac{\int [\epsilon(\mathbf{r}) - \tilde{\epsilon}(\mathbf{r})] |E_{n\mathbf{k}}(\mathbf{r})|^2 d\mathbf{r}}{\int \epsilon(\mathbf{r}) |E_{n\mathbf{k}}(\mathbf{r})|^2 d\mathbf{r}}. \quad (7)$$

From Eq. (7), we can estimate easily the shift in eigenfrequency before and after the insertion for s wave.

III. NUMERICAL RESULTS AND DISCUSSIONS

In this section, we will first compare the numerical results obtained from both the perturbative and multiple-scattering approaches in the case of dielectric insertion to show the validity of our method. Then we will use the perturbative approach as the guide to make metallic insertions. Our multiple-scattering results show that both full and complete gaps can be enlarged significantly. The system we considered here consists of an array of cylinders with dielectric constant ϵ_c in a background of dielectric constant ϵ_b . We denote the dielectric constant of the third component as ϵ_i . We first consider a situation discussed in Ref. 14. The original system consists of air cylinders ($\epsilon_c=1$) of radii R embedded in a background dielectric with $\epsilon_b=11.4$ in a square lattice with lattice constant a . The insertion is made by air cylinder ($\epsilon_i=1$) of radius R_i at the center of each unit cell. Thus, we have $\delta \equiv \epsilon_i^{-1} - \epsilon_b^{-1} \approx 0.91 > 0$. For the original system, we have used the multiple-scattering method to calculate the band structures $\omega_{n\mathbf{k}}$, eigenfields, and gap positions.^{9,15,16}

The calculated band structure of s wave in square lattice of air cylinder with $R/a=0.485$ is plotted in Fig. 1. In terms of the dimensionless frequency $\nu \equiv \omega a / 2\pi c$, the first gap

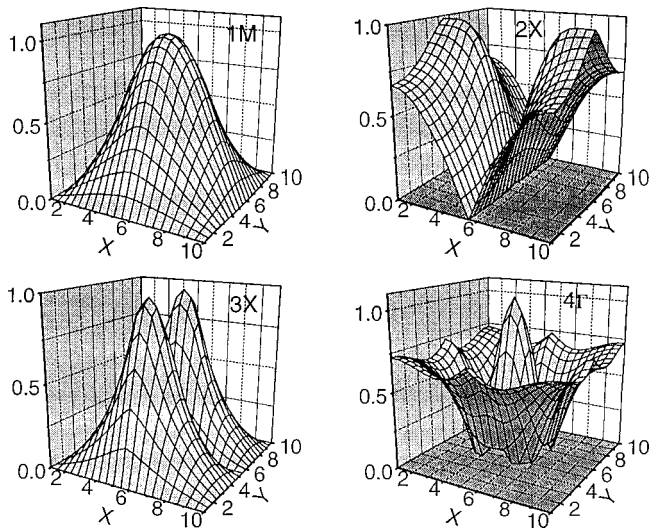


FIG. 2. In the case of *s* waves, distribution of the absolute value of the electric field (in arbitrary units) for four eigenstates at the band edges.

appears from $\nu_{1M} \cong 0.249$ to $\nu_{2X} \cong 0.314$, whereas the second gap appears from $\nu_{3X} \cong 0.450$ to $\nu_{4\Gamma} \cong 0.490$. At the same time, we also plot the function $|E_{nk}(\mathbf{r})|$ in a unit cell for the band-edge states 1M, 2X, 3X, and 4Γ in Fig. 2. The corners of the unit cell correspond to the centers of air cylinders. After the insertion of air cylinders at the center of each unit cell, we have estimated the gap position by using Eq. (7) and plot the results as the dashed and solid lines in Fig. 3(a) for the first and second gaps, respectively. Since the function $|E_{nk}(\mathbf{r})|$ has its minimum at the insertion position for states 2X and 3X, the upper edge of the first gap and the lower edge of the second gap remain unaffected. However, for the

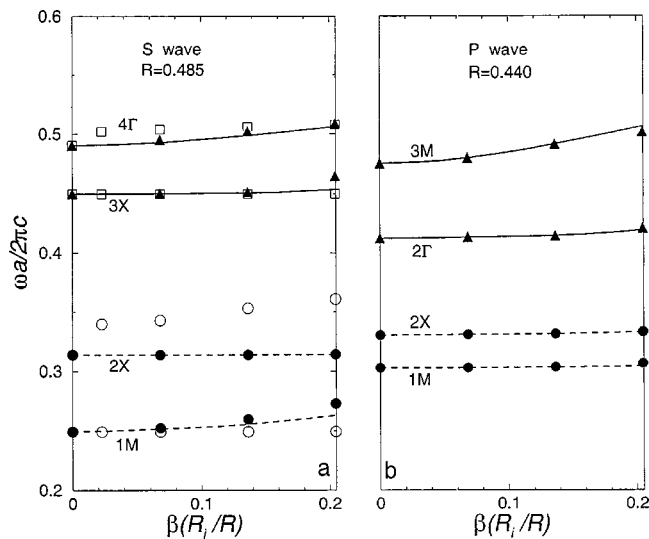


FIG. 3. Gap structures after the insertion of air cylinders of radii R_i at the center of each unit cell. The original system consists of air cylinders of radii R in a square lattice in a background dielectric ($\epsilon_b = 11.4$) (a) for *s* waves and (b) for *p* waves. The dashed and solid lines denote the estimated results for the first and second gaps, respectively. The solid circles and triangles denote the calculated gaps. The open circles and squares denote the calculated gaps for the insertion of metallic cylinders.

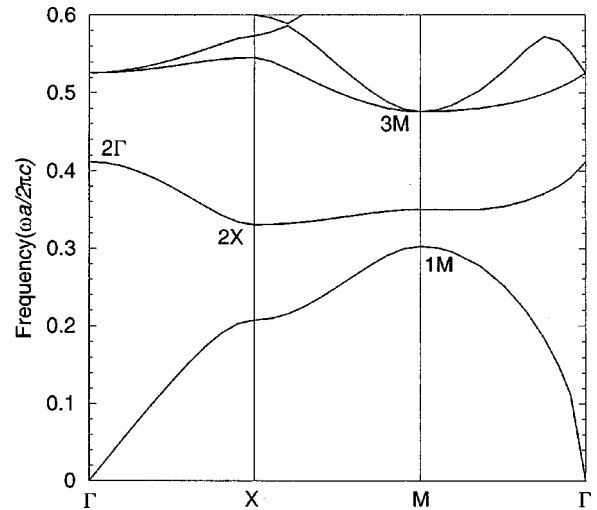


FIG. 4. Calculated photonic band structure of a *p* wave for a square lattice of an air cylinder with $R/a = 0.440$. The dielectric constant of background is taken as 11.4.

states at 1M and 4Γ, $|E_{nk}(\mathbf{r})|$ becomes a maximum at the insertion position. Thus, both the lower edge of the first gap and upper edge of the second gap increase with β . As a result, the first gap is reduced while the second gap is enlarged. For comparison, we also plot in Fig. 3(a) the calculated gap position obtained from the multiple-scattering approach by solid circles and triangles for the first and second gaps, respectively. The excellent agreement between the estimated and calculated results demonstrates the validity of the method and the accuracy of Eq. (7) when $\beta < 0.2$. When $\beta \geq 0.2$, discrepancies appear and Eq. (7) becomes invalid. At $\beta = 0.16$, our results also agree quantitatively with that obtained from band structure calculations presented in Ref. 14.

For the case of *p* waves, the magnetic field is parallel to the cylinder axis. We have chosen $R/a = 0.440$, a square lattice of an air cylinder, to calculate the band structures ω_{nk} and the function $|D_{nk}(\mathbf{r})|$, which are shown in Figs. 4 and 5, respectively. The band-structure calculations indicate that the

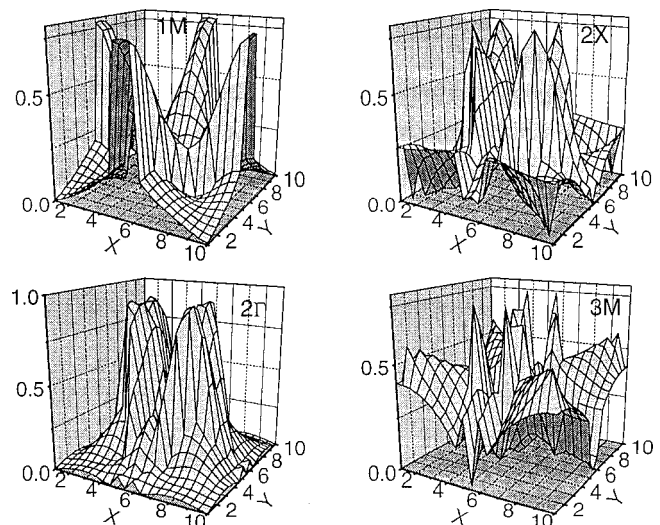


FIG. 5. In the case of *p* waves, distribution of the absolute value of the displacement field (in arbitrary units) for four eigenstates at the band edges.

first gap appears from $\nu_{1M} \cong 0.303$ to $\nu_{2X} \cong 0.332$ with the lower and upper band edges located at the states $1M$ and $2X$, respectively. The second gap appears from $\nu_{2\Gamma} \cong 0.412$ to $\nu_{3M} \cong 0.475$ with two edges located at 2Γ and $3M$. We have first used Eq. (5) to estimate the shifts in gap positions due to the insertion. The results are shown by two dashed and two solid lines in Fig. 3(b) for $\beta = R_i/R \leq 0.2$. The position of first gap is not much affected, whereas the second gap is enlarged due to the increase in eigenfrequency at the upper edge. These behaviors arise from the fact that the function $|D_{n\mathbf{k}}(\mathbf{r})|$ is at the minimum at the insertion position for the states $1M$, $2X$, and 2Γ , but it is at the maximum for the state $3M$. In Fig. 3(b), we also plot the calculated gap position by solid circles and triangles for the first and second gaps for comparison. We again find the excellent agreement between the estimated and calculated results for the case of p waves.

It should be mentioned that the enhancement in the second gap for s waves actually enlarges the absolute gap of the system.¹⁴ The reduction of the first gap can be understood by using the following simple arguments without knowing $|E_{n\mathbf{k}}(\mathbf{r})|$ explicitly. Since the first band is dielectric band, the state at the lower edge of the first gap will have an electric field concentrated near the center of the unit cell.² The insertion of the air cylinder will push the eigenfrequency up and reduce the gap. However, the second band is an air band with the electric field concentrated in air cylinders, and the eigenfrequency at the upper edge of the first gap will not be affected much by the insertion. Thus, we expect a reduction in the first gap, irrespective of the lattice structure. For higher-order gaps, the distinction between the dielectric and air bands becomes less obvious and an explicit form of $|E_{n\mathbf{k}}(\mathbf{r})|$ at two edges of the gap becomes necessary for an optimal insertion.

In order to enlarge the first gap, we should choose a different insertion. From Fig. 2, we observe that $|E_{n\mathbf{k}}(\mathbf{r})|$ is small for the state $1M$ at the center of the air cylinder, but it is large for the state $2X$. Thus, if we insert a cylinder with a negative dielectric constant at this position, the upper edge will shift to a higher frequency, while the lower one will remain unaffected as can be seen from Eq. (7). In fact, the same arguments apply to the states $3X$ and 4Γ at the band edges of the second gap. Thus, with such an insertion, both gaps can be enlarged at the same time. To confirm this, we insert a perfect conductor of radius R_i at the center of the air cylinder. The calculated gap position is now plotted as open circles and squares in Fig. 3(a) for the first and the second gaps, respectively. We find significant enlargements in both gaps even at a small β . It should be pointed out that we have also calculated the gap position by using a more realistic dielectric constant for the metal cylinder, i.e., $\epsilon_m = 1 - f_p^2/[f(f+i\gamma)]$, with the plasma frequency $f_p = 3600$ THz and absorption constant $\gamma = 340$ THz.^{10,15} For a wide range of structure (frequency) scales, i.e., from $a \approx 1$ mm (microwave) to $a \approx 1 \mu\text{m}$ (infrared), the gap position (in units of $\nu \equiv \omega a/2\pi c$) is close to that obtained from a perfect conductor.¹⁶ The sudden rise of gap size at a small β indicates that the gap can be significantly enlarged by the presence of only a small filling factor of the metal component. In this case, the effects due to absorption will be insignificant.

The metallic insertion at the center of the air cylinder is

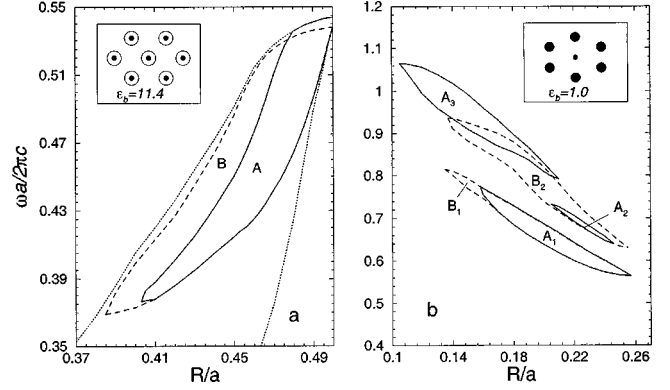


FIG. 6. (a) Gap map for triangular lattice of air cylinders in a background dielectric ($\epsilon_b = 11.4$). Region A denotes the absolute gap. The region surrounded by the dotted lines denotes the gap for p waves. Region B denotes the extension of the absolute gap from region A after the insertion of metallic cylinders of radii $R_i = 0.05a$ at the center of the air cylinders (inset). (b) Gap map for the honeycomb lattice of dielectric cylinders ($\epsilon_c = 11.4$) in air. Regions A_1 , A_2 , and A_3 denote absolute gaps. Regions B_1 and B_2 denote the extensions of the absolute gap from regions A_1 and A_2 after the insertion of metallic cylinders at the center of each honeycomb (inset).

particularly useful in the case of triangular lattice where the absolute gap appears as the first gap for s waves. The gap map for the system of a triangular array of air cylinders in a dielectric background $\epsilon_b = 11.4$ has been given in Ref. 2. In Fig. 6(a) we plot the gap map for the absolute gap with a solid line and denote it as region A. The region surrounded by two dotted lines represent the gap for p waves. After the insertion of a metal cylinder of radius $R_i = 0.05a$ at the center of the air cylinder, the region covered by the absolute gap extends from A to B. The gap structures for P waves are not much affected by the insertion. Thus, an absolute gap that appears as the primary gap can also be significantly enlarged by using this generalized method of insertion.

For the case of dielectric cylinders in air, we consider the honeycomb structure. When the dielectric constant of the cylinders is $\epsilon_c = 11.4$, three regions of absolute gaps have been found.² We denote them as A_1 , A_2 , and A_3 in Fig. 6(b). It has been shown that by using insertion of a dielectric cylinder at the center of each honeycomb, the third-order absolute gap A_3 can be enlarged.¹⁴ Here, we insert, instead of dielectric cylinders, metallic cylinders of radii $R_i = 0.05a$ at the center of each honeycomb. The regions covered by the first- and second-order absolute gaps have been extended from A_1 and A_2 to B_1 and B_2 , respectively. A significant enhancement of the second absolute gap is evident. It has been extended to the region covered by the third-order absolute gap of the original system. Thus, adopting the same insertion position, we are able to enlarge different absolute gaps by choosing different dielectric constants of the inserted component.

IV. EXPERIMENTAL DEMONSTRATION

In order to test our method experimentally, we have also carried out the following microwave experiments in the frequency range from 6.8 to 15.0 GHz. The transmittance of a

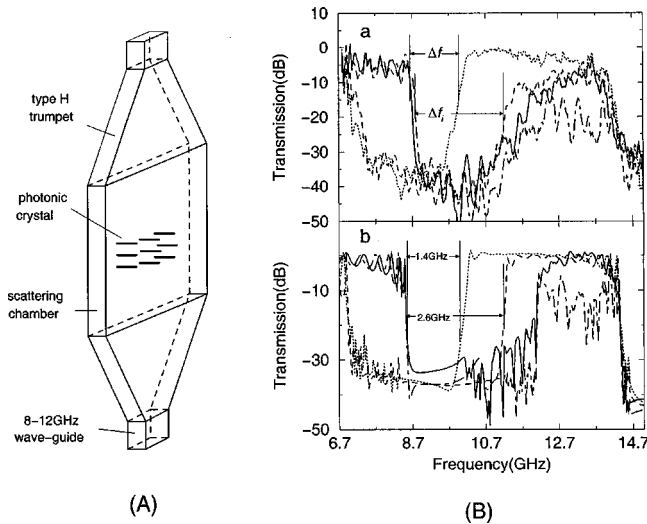


FIG. 7. (A) Schematic representation of the scattering system (not to scale); (B) parts (a) and (b) represent the measured and calculated transmission coefficients, respectively. For the original system of 10×23 dielectric cylinders ($\epsilon_c = 8.9$) of radii 3.03 ± 0.03 mm arranged in a square lattice in a styrofoam template, the dotted and solid curves denote results of normal (Γ - X) and oblique (Γ - M) incidences, respectively. After the insertion of metallic cylinders of radii 0.2 mm in the center of each unit cell, the corresponding results are denoted by the dashed and dot-dashed curves, respectively.

photonic crystal was measured in a two-dimensional wide waveguide scattering chamber. The chamber was composed of two components, the square groove and cover plate. The square groove with a 250 nm internal width, 270 mm external width, 350 mm length, and 10.16 mm depth was machined into a 20-mm-thick aluminum plate. The cover plate with a 270 mm width and a 350 mm length was machined into a 10-mm-thick aluminum plate. The inner surfaces of the chamber were polished to satisfy the requirement of the microwave measurement. To avoid the reflection from lateral wall of the chamber, its inner sides were furnished with a thick layer of low-density absorber. The back and forward ports of the chamber were fit in conjunction with the 8–12-GHz type- H trumpets of 350 mm in length. Then the trumpets were connected with standard 8–12-GHz waveguides. The PBG system was placed in the middle of the chamber. All of them consist of a complete device under test as shown in Fig. 7(A). The transmittance was measured by using an HP8757E scalar network analyzer and an HP8364A series synthesized sweeper.

The photonic crystal was composed of 10×23 alumina cylinders with dielectric constant 8.9 and radii 3.03 ± 0.03 mm embedded in a styrofoam template, arranged in a square lattice with a lattice constant 9 mm. The normal surface of the photonic crystal corresponded to the Γ - X direction in the first Brillouin zone. Meanwhile, we also fabricated three metallodielectric photonic crystals by inserting copper cylinders of 0.2, 0.3, and 0.4 mm radii into the center of each square of the dielectric photonic crystal. For a better simulation of the infinite photonic crystal in the traverse direction, a 7-cm-wide slit was placed in the front of the photonic crystal. In part (a) of Fig. 7(B), we plot the measured transmission data. The dashed and dotted curves are the re-

sults of normal incidence (Γ - X) for the cases of with and without 0.2-mm ($\beta \approx 0.067$) metal cylinders, respectively. The corresponding results for the case of oblique incidence (Γ - M) are shown as the dot-dashed and solid curves, respectively. We calculated the transmission coefficients for the above cases by using the multiple-scattering method.¹⁵ The corresponding theoretical results are shown in part (b) of Fig. 7(B). Both experiment and theory have shown that the (full) gap width is nearly doubled from the original width $\Delta f \approx 1.4$ GHz to $\Delta f_i \approx 2.6$ GHz after the insertion of metallic cylinders. Their discrepancies in the pass band may be due to the misalignment of cylinders as well as other disorder effects in the sample. Although the experiments were carried out in the microwave region, we have also calculated the transmission near the optical regime by rescaling the lattice constant from $a = 9$ mm to $0.9 \mu\text{m}$. From its size dependence, we determine that the absorption length in the pass band shown in Fig. 7(B) to be about $40a$. Such a large decay length is a result of small filling factor (≈ 0.0015) of the metallic component. Thus, unlike metallic photonic crystals, a metallic insertion into a dielectric photonic crystal can have large gap with small absorption and be useful in applications.

V. CONCLUSION

In this paper, we have proposed a simple, systematic, and efficient method to enlarge the gap of a photonic crystal. In this method, we add a small fraction of a third component into the existing photonic crystal. Based on a perturbation analysis, the dielectric property of the third component as well as its insertion position in a unit cell are chosen according to the field-energy distribution of two Bloch states at the band edges. The field distributions at band edges have been calculated by the multiple-scattering method and their structures can be understood from the variational principle. In the case of dielectric insertion, the excellent agreement between the perturbative analysis and multiple-scattering results shows the validity of our method. Thus, the perturbative approach can provide us an efficient way in the choices of the dielectric property of the insertion as well as the insertion position to enlarge PBG's, whereas the gap structure of the altered microstructure should be obtained from more accurate calculations such as the multiple-scattering method. By doing so, in the case of metallic insertion, we are able to obtain much larger full and complete gaps. An explicit experimental demonstration of the method in the microwave region is also presented. Our method is very general and it does not require symmetry breaking. Although we have considered here only a few simple microstructures in 2D, nevertheless, the method proposed here can be applied to all microstructures in 2D and 3D photonic crystals.^{5–8,11,12} In 3D, since all waves are vector waves, Eq. (5) should be used to estimate the frequency shift. Thus, our method opens up a new way to engineer photonic band gaps.

ACKNOWLEDGMENTS

The authors thank C. T. Chan and P. Sheng for discussions. The work was supported by Hong Kong RGC Grant No. HKUST 6112/98P and the National Natural Science Foundation of China.

- ¹*Photonic Band Gap Materials*, edited by C. M. Soukoulis (Kluwer Academic, Dordrecht, 1996); E. Yablonovitch, *Phys. Rev. Lett.* **58**, 2059 (1987); S. John, *ibid.* **58**, 2486 (1987); K. M. Ho, C. T. Chan, and C. M. Soukoulis, *ibid.* **65**, 3152 (1990).
- ²J. D. Joannopoulos, R. D. Meade, and J. N. Winn, *Photonic Crystal-Molding the Flow of Light* (Princeton University Press, Princeton, NJ, 1995).
- ³S. L. McCall *et al.*, *Phys. Rev. Lett.* **67**, 2017 (1991).
- ⁴W. M. Robertson *et al.*, *Phys. Rev. Lett.* **68**, 2023 (1992).
- ⁵E. Yabonovitch, *J. Opt. Soc. Am. B* **10**, 283 (1993).
- ⁶T. F. Krauss, R. M. De La Rue, and S. Brand, *Nature (London)* **383**, 699 (1996).
- ⁷D. Labilloy *et al.*, *Phys. Rev. Lett.* **79**, 4147 (1997).
- ⁸S. Y. Lin *et al.*, *Nature (London)* **394**, 251 (1998).
- ⁹N. A. Nicorovici, R. C. McPhedran, and L. C. Botten, *Phys. Rev. B* **52**, 1135 (1995).
- ¹⁰M. M. Sigalas, C. T. Chan, K. M. Ho, and C. M. Soukoulis, *Phys. Rev. B* **52**, 11 744 (1995).
- ¹¹D. F. Sievenpiper, M. E. Sickmiller, and E. Yablonovitch, *Phys. Rev. Lett.* **76**, 2480 (1996).
- ¹²D. F. Sievenpiper *et al.*, *Phys. Rev. Lett.* **80**, 2829 (1998).
- ¹³K. A. McIntosh *et al.*, *Appl. Phys. Lett.* **70**, 2937 (1997).
- ¹⁴C. M. Anderson and K. P. Giapis, *Phys. Rev. Lett.* **77**, 2949 (1996); *Phys. Rev. B* **56**, 7313 (1997).
- ¹⁵L. M. Li and Z. Q. Zhang, *Phys. Rev. B* **58**, 9587 (1998).
- ¹⁶L. M. Li, Z. Q. Zhang, and X. Zhang, *Phys. Rev. B* **58**, 15 589 (1998).